

Template Synthesis of Nitrogen Self-Doped Hierarchical Porous Carbon with Supermicropores and Mesopores for Electrical Double-Layer Capacitors

Xiaodan Yuan,^a Liwen Xu,^a Jubing Zhang,^a Yun Dai,^b Juguang Meng,^a Xinye Wang,^a Changsheng Bu,^a Changqi Liu,^a and Hao Xie^{a,*}

Nitrogen self-doped hierarchical porous carbon for electrical double-layer capacitors was synthesized by direct carbonization of bean dregs-based tar with potassium acetate as the template agent. The pore structure parameters and chemical element composition were adjusted by varying the heating rate during the carbonization process. The electrochemical properties of the electrode materials were evaluated in a three electrode system with 6 M KOH as the electrolyte. The resultant bean dregs-based porous carbons (BDPCs) exhibited high specific surface area, unique hierarchical architecture (consisting of supermicro- and mesopores), and medium nitrogen content (0.66 to 0.78%). The BDPC-10 sample had the highest specific surface area of 1610 m²/g and reasonable pore size distribution, and consequently exhibited an excellent specific capacitance of 363.7 F/g at the current density of 1 A/g. Nevertheless, the capacitance was reduced to 280.5 F/g at 3 A/g, giving a capacitance retention ratio of 77.1%. This study suggests a facile and environmentally friendly template synthesis process for supercapacitor electrode materials preparation, but it also faces challenges to increase the rate capability.

DOI: 10.15376/biores.18.1.87-99

Keywords: Bean dregs; Template; Hierarchical porous carbon; Electrical double-layer capacitor; Supermicropore

Contact information: a: School of Energy and Mechanical Engineering, Nanjing Normal University, Nanjing, 210042, China; b: Jiangsu Nantong Power Generation Co., Ltd, Nantong, 226005, China; *Corresponding author: xhylon@163.com

INTRODUCTION

Due to their high power density, fast charging/discharging rate, and excellent cycling stability, supercapacitors have been used for portable electronics, hybrid electric vehicles, new energy power generation system, and other large industrial scale systems (Borenstein *et al.* 2017; Chen *et al.* 2018; Poonam *et al.* 2019). Supercapacitors are divided into electrical double-layer capacitors (EDLCs) and faradaic pseudocapacitors based on the differences in working mechanism; most commercially available supercapacitor devices contain EDLCs (González *et al.* 2016; Simon and Gogotsi 2020). Because EDLCs store electrical energy by accumulating charge at the electrode/electrolyte interfaces, high surface area is an essential requirement for electrode materials to provide enough adsorption sites (Niu *et al.* 2017; Zhang *et al.* 2018).

Pores in powder materials can be classified into three categories, micropores ($d < 2$ nm), mesopores ($2 \text{ nm} < d < 50$ nm), and macropores ($d > 50$ nm). Micropores greatly increase the accessible surface area for ion charge accommodation and contribute to high

capacitive properties. Mesopores provide transport highways for ions diffusing to the inner surface of electrode materials, while macropores act as buffering reservoirs to reduce ion transport distance (Miao *et al.* 2018). Mesopores and micropores play crucial roles in the electrochemical behaviors of EDLCs. The micropores have two subgroups of ultramicropores ($d < 0.7$ nm) and supermicropores ($0.7 \text{ nm} < d < 2$ nm). Micropores with too small size reduce the conductivity and deteriorate rate capability, while even making no contribution to electrical double-layer capacitance under certain conditions (Lin *et al.* 1999; Wen *et al.* 2005; Jin *et al.* 2011). As a result, a reasonable pore size distribution (PZD) is a critical parameter for electrode materials.

Carbonaceous materials, such as activated carbon, carbon nanotube, graphene, and carbon aerogel are promising candidates for EDLCs because of their well developed pore structure, fast kinetics, high electrical conductivity, and stable physical and chemical properties. Among them, activated carbon is the most widely used carbon-based electrode material due to its low cost and extra high surface area (Wang *et al.* 2012; Gao *et al.* 2021). To improve the capacitive properties of EDLCs, one promising approach is using carbon materials with well-balanced hierarchical nanoarchitecture, which can take the merits of each pore size via a synergistic action during charging/discharging process. Commercial activated carbon with high surface area is prepared through physical/chemical activation. However, it is difficult to control PZD during the activation because it is very sensitive to reaction conditions. In contrast, the template synthesis method easily regulates the PZD by using different template agents and adjusting the amount of template in relation to the carbon precursor (Xiao *et al.* 2017; Tang *et al.* 2018; Zhang *et al.* 2021).

Heteroatoms doping is another efficient way to improve the electrochemical performance. The introduction of heteroatoms (N, O, S) into carbon matrix transform the electric and crystalline structures of target carbons and enhance chemical stability, surface polarity, electrical conductivity, and electron-donor properties, which stimulates additional pseudocapacitance (Zhao *et al.* 2018). Nitrogen is the most common dopant, and nitrogen doping is achieved *via* post-treatment of carbon materials in nitrogen-containing media or by direct carbonization of nitrogen containing precursors (Lin *et al.* 2015; Li *et al.* 2016). Due to the advantages of homogeneous heteroatom distribution, controlled dopant content, and stable porosity, the self-doping strategy has gradually replaced the post-treatment strategy (Liu *et al.* 2016; Song *et al.* 2020).

A simple and efficient synthesis of nitrogen self-doped hierarchical porous carbons (HPCs) with supermicropores and mesopores is highly attractive for EDLCs, but it remains challenging. Most HPCs obtained from hard/soft templating method lack micropores; additional post-activation is used to generate micropores and enlarge specific surface area. Simultaneously, template removal and post-activation process involve environmental unfriendly conditions, such as acid washing and alkali etching. With the increasing concern about pollution, there is a strong global interest in renewable resources as alternative feedstocks for carbon materials production (Chen *et al.* 2017; Yi *et al.* 2020; Zhang *et al.* 2021). Thus, HPCs prepared for EDLCs with biomass precursor have gained attention.

This study reports a novel template synthesis of nitrogen self-doped HPCs via direct carbonization of nitrogen-rich bio-tar with potassium acetate as the salt template. The bio-tar was derived from bean-dregs pyrolysis, serving as both carbon source and nitrogen source. Potassium acetate acted as template to form initial pores, and its decomposition products generated secondary pore structures. The template agent was removed easily by water washing. The capacitive properties of the prepared HPCs were studied in 6M KOH electrolyte. The resulting HPCs possessed large specific surface area, unique porous

nanoarchitecture (uniform supermicropores and mesopores), and a medium amount of nitrogen dopant. The HPC-10 sample displayed an excellent high specific capacitance of 363.7 F/g at the current density of 1 A/g.

EXPERIMENTAL

Synthesis of Carbon Samples

Bean dregs (the soybean residue after soybean milk squeezing) were provided by a soybean processing plant in Nanjing City. The proximate analysis and elemental analysis of bean dregs are summarized in Table 1. The bean dregs with the particle size of about 20 mesh were pyrolyzed in nitrogen flow with the terminal temperature of 800 °C and heating rate of 20 °C/min. The pyrolysis gas was cooled in ice bath, and ethanol was added dropwise into the condensate until the water insolubles were entirely dissolved. The mixture was filtered with filter paper to remove residual raw material and coke, and bean dregs-based tar (BDT) was obtained by evaporating the filtrate adequately at 80 °C.

Table 1. Proximate Analysis and Elemental Analysis of Bean Dregs

Sample	Proximate Analysis (%)				Elemental Analysis (%)			
	M _{ad}	V _{ad}	A _{ad}	FC _{ad}	C _{ad}	H _{ad}	N _{ad}	O _{ad}
Bean dregs	9.33	71.85	5.15	13.67	48.54	7.60	9.53	19.85

The HPC was synthesized by the direct pyrolysis of precursor (the mixture of BDT and potassium acetate). Typically, 10 g of potassium acetate was added into 15 mL of deionized water and the liquid was heated to 95 °C in water bath. Then, 1 g of agar (curing agent) was added into this solution with magnetic stirring for 0.5 h. Into this mixture, 2.5 g of BDT dissolved in 15 mL of ethanol was added with adequate mixing. The resultant precursor was solidified in ice water and then dried at 40 °C for 48 h in a drying oven. The dried precursor was carbonized at 800 °C under nitrogen flow with different heating rates. Finally, bean dregs-based porous carbons (denoted as BDPC-x, where x refers to the heating rate) were obtained by removing template agent from carbonized samples with deionized water washing.

Characterization

Nitrogen adsorption-desorption isotherms at 77 K were measured using an ASAP 2460 surface area and pore size analyzer (Micromeritics, Norcross, GA, USA). The specific surface area and pore size distribution were obtained by the Brunauer-Emmett-Teller method and nonlocal density functional theory equilibrium model, respectively. The structure was analyzed by X-ray diffraction method (D8 Advance, Bruker, Karlsruhe, Germany) equipped with Cu radiation ($\lambda = 0.154$ nm). Fourier transform infrared (FT-IR) spectra were recorded under identical conditions in the range of 400 to 4000 cm^{-1} with a Nicolet IS10 spectrometer (Thermo Fisher, Waltham, America). Elemental analysis was performed on an elemental analyzer (EA 3000, Euro Vector, Stuttgart, Italy). The chemical element composition and nitrogen valence were investigated on an X-ray photoelectron spectrometer (Escalab 250Xi, Thermo Fisher, Waltham, America).

Electrochemical Measurements

The BDPC powder prepared above (3 mg) was mixed with polytetrafluoroethylene (PTFE) binder and acetylene black according to the mass ratio of 8:1:1 and then dispersed in ethanol solvent to form a slurry. The slurry was dried at 60 °C overnight to form a dough and rolled into a rounded slice. The working electrode was assembled by pressing the slice onto nickel foam under 10 MPa and dried at 100 °C to eliminate residual solvent.

Electrochemical measurements were carried out on a CHI660E electrochemical workstation (Chinstruments, Shanghai, China) in three electrode system with 6M KOH aqueous solution as the electrolyte. A platinum plate electrode (2 cm × 2 cm) and Hg/HgO electrode were utilized as the counter electrode and reference electrode, respectively. Cyclic voltammetry (CV) was scanned in the range of -0.9 to 0 V (vs. Hg/HgO) at different scanning rates. The galvanostatic charge-discharge (GCD) experiments were performed in the same potential range at different current densities. Electrochemical impedance spectroscopy (EIS) was measured in the frequency range from 100 kHz to 0.01 Hz. The gravimetric specific capacitance was calculated using Eq. 1,

$$C_m = \frac{I \times \Delta t}{\Delta V \times m} \quad (1)$$

where C_m is the gravimetric specific capacitance (F/g), I is the discharge current (A), Δt is the discharge time (s), ΔV is the potential window (V) during the discharge process, and m is the mass of electroactive materials in the working electrode (g).

RESULTS AND DISCUSSION

Nitrogen adsorption-desorption isotherms at 77 K and the corresponding pore size distribution curves of the as prepared BDPCs are illustrated in Fig. 1. The primary pore structure parameters, including specific surface area, pore volume, and pore diameter are listed in Table 1.

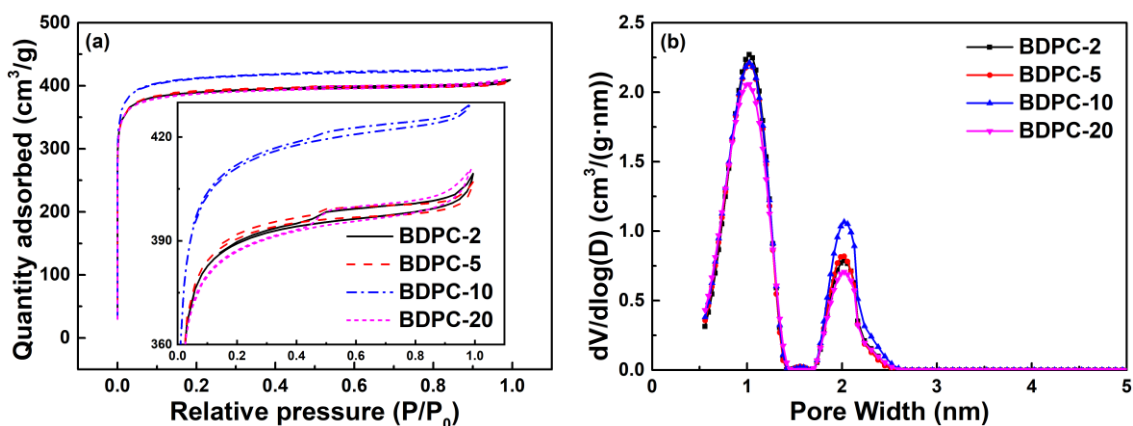


Fig. 1. N₂ adsorption-desorption isotherms (a) and pore size distribution curves (b) of BDPCs

The adsorption isotherms (Fig.1a) shows a sharp increase in adsorbed volume at $P/P_0 < 0.05$, revealing typical type I characteristic feature, which implies that the BDPCs were rich in micropores. Meanwhile, a small hysteresis loop at medium relative pressure can be observed, which is ascribed to the presence of small sized mesopores (Du *et al.* 2017). As shown in Fig. 1b, BDPCs exhibited two different scales of pores,

supermicropores and small sized mesopores, concentrated at 1.05 and 2.05 nm, respectively. Potassium acetate disperses uniformly in the precursor because of its high solubility in water and crystallizes as tiny particles during the precursor pyrolysis process. Small sized mesopores and some supermicropores are released after removing the template. Additionally, abundant micropores are produced by the *in-situ* activation of K_2CO_3 , CO_2 , and H_2O derived from the pyrolysis process of precursor (Zhang *et al.* 2017). According to the detailed pore structure parameters listed in Table 2, all of the BDPCs were classified as micropore carbons due to their extremely high microporosities. As the heating rate increased from 2 to 20 °C/min, both the specific surface area and the total pore volume first increased and then decreased, while the average pore width barely changed. BDPC-10 showed the highest specific surface area of 1610 m^2/g and the largest total pore volume of 0.66 cm^3/g .

Table 2. Porosity Parameters of BDPC Samples

samples	S_{BET}	S_{micro}	V_{total}	V_{micro}	V_{micro} / V_{total}	$D_{average}$
	m^2/g		cm^3/g		%	nm
BDPC-2	130	1450	0.63	0.51	94.77	1.64
BDPC-5	1540	1470	0.63	0.50	95.45	1.64
BDPC-10	1610	1460	0.66	0.51	90.68	1.66
BDPC-20	1190	1060	0.52	0.50	89.08	1.69

XRD patterns were used to evaluate the structure of the BDPC, as shown in Fig. 2a. In the XRD patterns, all of the BDPCs displayed a broadened diffraction peak located at 26° and a weak diffraction peak situated at 44°, which are assigned to the (002) and (100) diffraction peaks of graphitic type lattice, respectively. This implies that all BDPCs had amorphous structure, but with a certain degree of graphitization (Zhang *et al.* 2017; Jiang *et al.* 2022). With the increase in heating rate, the diffraction peaks become sharp, and the diffraction peak corresponding to the (002) plane shifted to a lower diffraction angle, indicating a deterioration in the graphitization of BDPC (Liu *et al.* 2018), and the decrease in graphitization further results in the decrease of electrical conductivity (Shu *et al.* 2020; Shilpa *et al.* 2016).

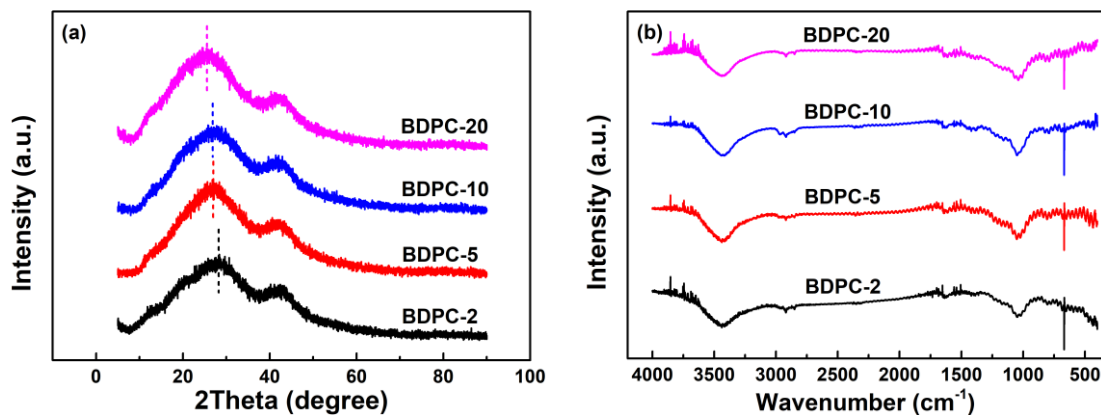
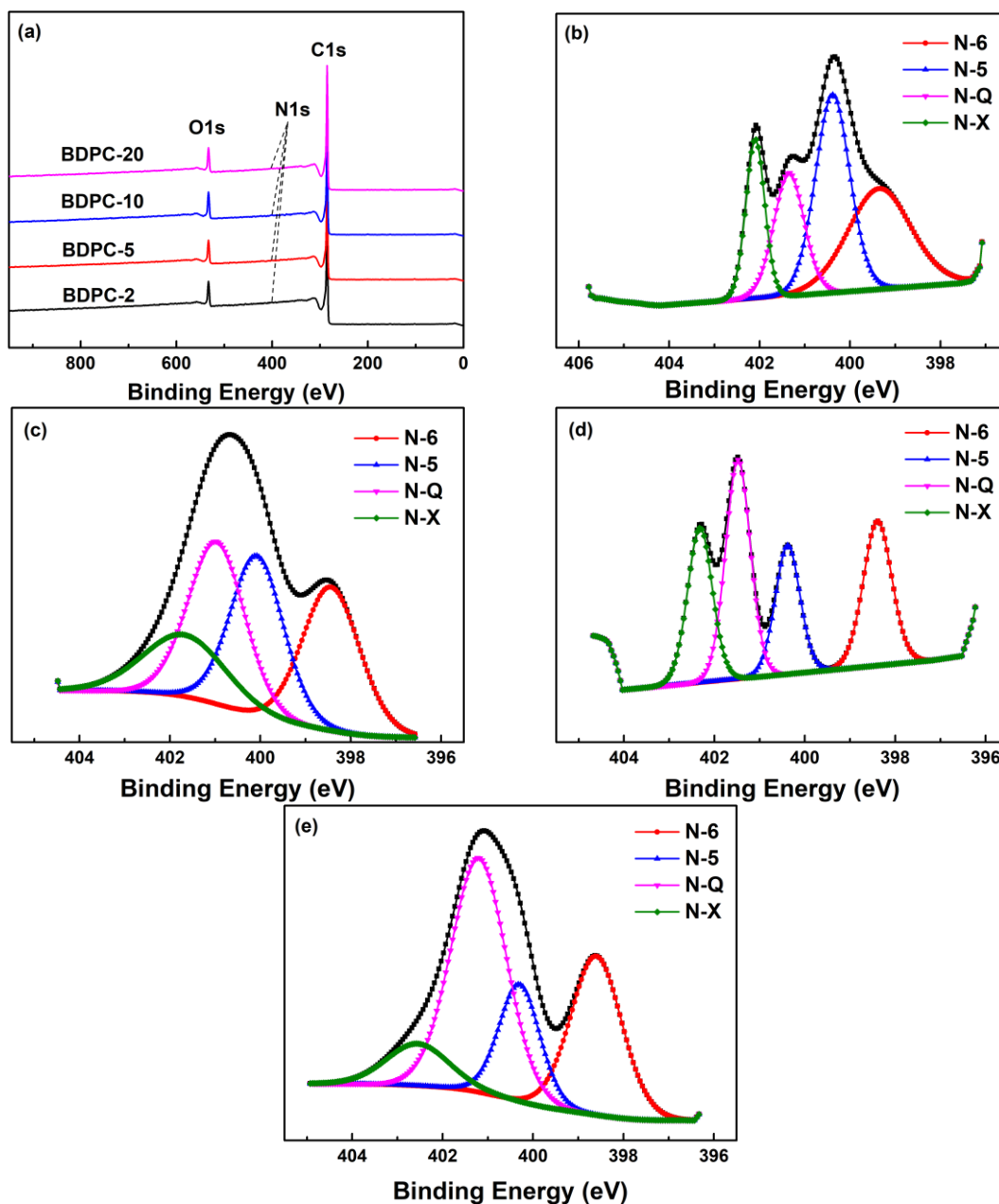


Fig. 2. XRD patterns (a) and FT-IR spectra (b) for BDPCs

FT-IR (Fig. 2b) was utilized to characterize the surface functional groups in BDPC samples prepared at different heating rates.

Table 3. Composition of BDPCs by EA and XPS

sample	EA (wt%)				XPS (at%)
	C	H	N	O	N
BDPC-2	60.42	2.75	0.78	36.05	0.72
BDPC-5	64.47	2.50	0.76	32.27	0.75
BDPC-10	67.05	2.58	0.70	29.67	0.81
BDPC-20	68.51	2.55	0.66	28.28	0.63

**Fig. 3.** XPS survey spectra (a); high-resolution N1s for BDPC-2 (b), BDPC-5 (c), BDPC-10 (d) and BDPC-20 (e)

Obviously, the FT-IR spectra displayed a similar shape, accompanied with the following diffraction peaks: the broad peak at about 3430 cm^{-1} attributed to the stretching

vibrations of O-H and/or N-H; the peak around 2850 cm^{-1} assigned to C-H stretching vibration in alkyl compounds; the peak located at about 1620 cm^{-1} ascribed to the C=C stretching vibration in the aromatic ring, the C=N stretching vibration in the triazine ring of melamine, and -NO₂ stretching vibration in nitro compounds; and the peak at about 1030 cm^{-1} due to the C-O stretching vibration or C-H bending vibration (Xu *et al.* 2021; Yakaboylu *et al.* 2021). According to the FT-IR spectra, all BDPCs contained certain amounts of oxygen and nitrogen functional groups. The redox reactions of these functional groups could bring additional pseudocapacitance.

The elemental composition of BDPCs derived from elemental analysis is listed in Table 3. The N content in BDT was 4.55% according to an earlier study, and thus it was used as the carbon and nitrogen source in this study. The BDPCs prepared at different heating rates exhibited relatively low N content, less than 1%. This result suggests that nitrogen-containing light components escaped from the BDT during the carbonization, resulting in low N content in BDPCs. The byproduct derived from agar pyrolysis further reduced the N content. As the heating rate was increased from 2 to 20 $^{\circ}\text{C}/\text{min}$, the N content decreased from 0.78 to 0.66 wt% gradually because high heating rate accelerated the loss of N element due to the lower bond energy of the C-N covalent bond (305 kJ/mol) compared to that of the C-C covalent bond (347 kJ/mol).

The XPS spectra displayed two peaks at the binding energies of 285 and 533 eV (Fig. 3a), which are assigned to C1s and O1s, respectively. In addition, an inconspicuous peak at the binding energy of 400 eV ascribed to N1s was identified. The N content calculated from XPS (Table 2) was similar to that obtained by EA analysis, revealing that the N element was uniformly distributed in the BDPCs. High resolution XPS spectra were further performed to investigate the chemical states of N-species in BDPC samples (Fig. 3b-d). The N1s XPS spectra could be deconvoluted into four peaks centered at 398.4, 400.5, 401.0, and 402.6 eV, which correspond to pyridinic N (N-6), pyrrolic N (N-5), graphitic N (N-Q), and pyridine N-oxide (N-X), respectively (Miao *et al.* 2018). As reported previously, N-5 is formed by an N atom contributing two p-electrons to the π -conjugated system, which can reinforce the activity for electrons and also facilitate the transportation and diffusion of electrolyte ions. N-6 is usually located at the edges of graphene layers by substituting a carbon atom on the C6 ring, and consequently acting as an electron donor. N-Q is embedded in the central region of the graphene layers (Song *et al.* 2020). N-5 and N-6 are conducive to increase the faradaic pseudocapacitance, while N-Q is beneficial to enhance the electronic conductivity. However, the detailed electrochemical mechanisms of N-X and N-Q are unclear.

The percentages of N-species accounting for the total N content in BDPCs are summarized in Table 4. With the increase in heating rate, the percentages of N-6 and N-5 decrease gradually, but the percentage of N-Q increases rapidly. The introduction of N improves the wettability of BDPCs and increases the surface availability, but it enhances faradaic pseudocapacitance (Yakaboylu *et al.* 2021).

Table 4. Percentage of N-species in BDPC Samples

N-species	BDPC-2	BDPC-5	BDPC-10	BDPC-20
N-6	22.66	25.21	24.80	22.40
N-5	32.78	27.34	20.25	11.60
N-Q	17.68	26.65	32.78	47.22
N-X	26.88	21.8	22.17	18.78

The CV curves of BDPC electrodes obtained at the scanning rate of 5 mV/s over the potential window of -0.9-0V (vs. Hg/HgO) are shown in Fig. 4a. All the CV curves displayed the quasi-rectangular shape without apparent redox peaks, demonstrating that the capacitance was basically provided by electrical double-layer electrostatic adsorption (Fiset *et al.* 2015; Miao *et al.* 2018). It is speculated that most oxygen/nitrogen functional groups could not be electrochemically oxidized/reduced or the redox reaction rates were too slow in the potential window. As a result, the pseudocapacitance was very small relative to the electrical double-layer capacitance, leading to no apparent redox peaks in the CV curves. BDPC-10 shows the largest integrated area in CV curves, followed by BDPC-5, BDPC-2 and BDPC-20 in sequence, which indicates that BDPC-10 possessed the highest specific capacitance among the tested BDPC electrodes (Miao *et al.* 2018). The CV curves of BDPC-10 with the scanning rate range from 5 to 100 mV/s are depicted in Fig. 4b. As the scanning rate was increased, the profiles maintained a roughly rectangular shape except for an increasingly apparent distortion, indicating an increased diffusion resistance at a high scanning rate. It is deduced that the diffusion of electrolyte ions at high scanning rate may be restricted by the relatively narrow pore channel attributed to the small sized mesopores (Ren *et al.* 2022).

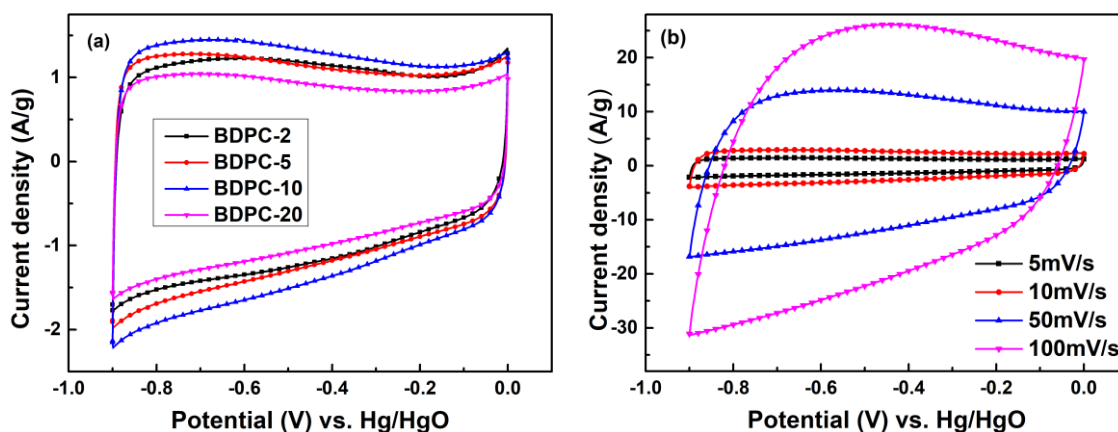


Fig. 4. CV curves of BDPC electrodes at a scanning rate of 5 mV/s (a) and BDPC-10 electrode at various scan rates (b)

The GCD profiles of BDPC electrodes obtained at the current density of 1 A/g over the potential window of -0.9 to 0.1 V (vs. Hg/HgO) are shown in Fig. 5a. The linear discharge branch further manifests the electrical double-layer characteristics of BDPC electrodes. A clear transition occurred at -0.1V in charge curve, which is assigned to the limited diffusion rate of ions.

The calculated specific capacitances at 1 A/g according to discharge curves decreased in the following order: BDPC-10 (363.7 F/g) > BDPC-5 (341.8 F/g) > BDPC-2 (328.9 F/g) > BDPC-20 (321.1 F/g), which agreed with the CV analysis. Though BDPC-10 had a lower heteroatom content than those of BDPC-2 and BDPC-5, it showed higher specific capacitance because of its large specific surface area (Song *et al.* 2019), well-balanced hierarchical nanoarchitecture, and high electron conductivity. BDPC-10 was further tested in a large range of current density (Fig. 5b). The specific capacitances at 1, 2 and 3 A/g were calculated as 363.7, 297.8, and 280.5 F/g, respectively, indicating a slightly poor rate capability. The diffusion of electrolyte ions in small sized mesopores (about 2

nm) become more difficult at high charge/discharge rate, resulting in a rapid decrease in specific capacitance (Wang *et al.* 2020).

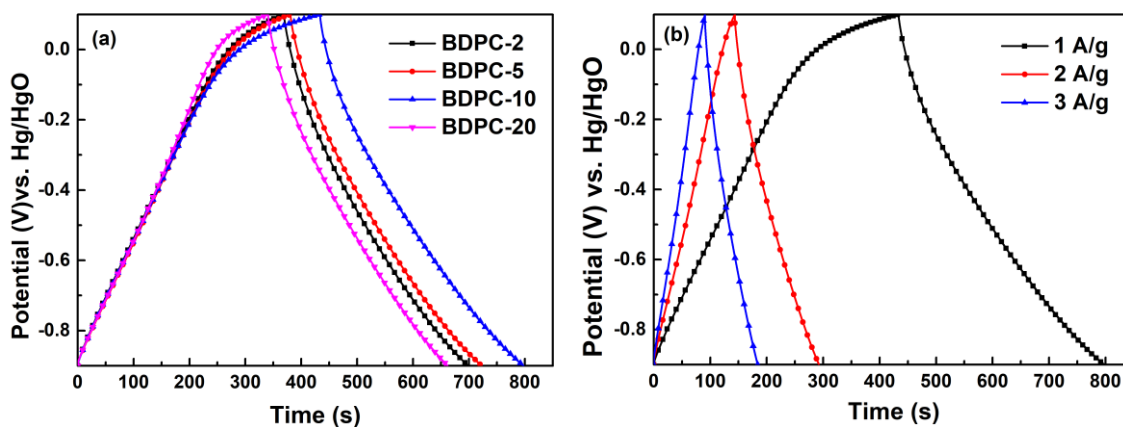


Fig. 5. GCD curves of BDPC electrodes at the current density of 1 A/g (a) and BDPC-10 electrode at various current densities (b)

EIS measurement was applied to investigate the electrochemical reaction kinetics in BDPC electrodes, and the Nyquist plots are illustrated in Fig. 6.

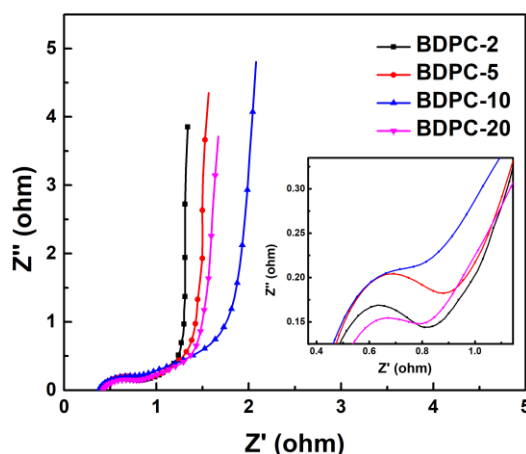


Fig. 6. EIS curves of BDPC electrodes

Each Nyquist plot consists of three parts: a semicircle (typically in the range of Z' equal to about 0.5 to 0.8 ohms), which is not completed during the electrochemical test in the high frequency region, a 45° diagonal line in the intermediate frequency region, and a vertical line in the low frequency region. The intercept on the real axis (Z') represents the equivalent series resistances (R_s), including electrode electronic resistance, electrolyte ionic resistance, and contact resistance at the electrode/electrolyte interface. BDPC-10 possessed the lowest R_s value of 0.375Ω among the samples (0.389 , 0.381 , and 0.423Ω for BDPC-2, BDPC-5, and BDPC-20, respectively), which can be primarily ascribed to its well developed pore structure serving as highways for electrolyte ions and high N-Q content accelerating electron transfer. The semicircle in high frequency can be attributed to the charge transfer process at the electrode/electrolyte interface. The diameter of the semicircle can be used to quantitatively analyze the charge transfer resistance (R_{ct}) of the BDPC electrodes and the difference in diameter can be assigned to the pseudotransfer

resistance. As the heating rate went up, the diameter became reduced gradually, indicating a downward trend in pseudotransfer resistance. This was attributed to the decreasing N content in BDPC-x, which is consistent with EA analysis. The slope of the straight line at the intermediate frequency corresponds to the Warburg diffusion resistance, which represents the diffusion/transport rate of electrolyte ions through the pores in the carbon electrode (He *et al.* 2019; Zhou *et al.* 2020). It is clear that all the intermediate frequency lines were closer to the vertical direction, indicating low diffusion resistance and good electrochemical capacitive properties. The EIS results further demonstrate that BDPCs had good electrical conductivity and the ability to transport electrons, which was consistent with the CV and GCD results (Yi *et al.* 2020).

CONCLUSIONS

1. The prepared bean dregs-based porous carbons at specified heating rates (BDPC-x) possessed high specific surface area (as high as 1610 m²/g), hierarchical nanoarchitecture (supermicro- and mesopores concentrated at 1.05 and 2.05 nm, respectively) and medium nitrogen content of 0.66 to 0.78%.
2. The cyclic voltammetry (CV) and galvanostatic charge-discharge (GCD) curves of BDPC-x displayed the quasi-rectangular shape and the isosceles triangular shape, respectively, indicating the electrical double-layer capacitive behavior.
3. The BDPC-10 showed the largest specific surface area of 1610 m²/g and optimized pore structure, and consequently exhibited an excellent specific capacitance of 363.7 F/g at 1 A/g in 6M KOH electrolyte.

ACKNOWLEDGMENTS

The authors are grateful for the support of the National Natural Science Foundation of China (51806110, 52106252), China Postdoctoral Science Foundation (2017M611858) and Jiangsu Provincial Natural Science Foundation of Jiangsu Province (BK20200733).

REFERENCES CITED

- Borenstein, A., Hanna, O., Attias, R., Luski, S., Brousse, T., and Aurbach, D. (2017). "Carbon-based composite materials for supercapacitor electrodes: A review," *J. Mater. Chem. A* 5(25), 12653-12672. DOI: 10.1039/c7ta00863e
- Chen, C., Zhang, Y., Li, Y., Dai, J., Song, J., Yao, Y., Gong, Y., Kierzewski, I., Xie, J. and Hu, L. (2017). "All-wood, low tortuosity, aqueous, biodegradable supercapacitors with ultra-high capacitance," *Energ. Environ. Sci.* 10(2), 538-545. DOI: 10.1039/c6ee03716j
- Chen, T., Luo, L., Li, Z., Zhang, Z., Zheng, S., Zhu, Z., He, J., and Zhao, W. (2018). "Preparation and characterization of nitrogen and oxygen heteroatom codoped activated biocarbons from edamame shell," *BioResources* 13(2), 3932-3948. DOI: 10.15376/biores.13.2.3932-3948

- Du, G., Bian, Q., Zhang, J., and Yang, X. (2017). "Facile fabrication of hierarchical porous carbon for a high-performance electrochemical capacitor," *RSC Advances* 7(73), 46329-46335. DOI: 10.1039/c7ra08402a
- Fiset, E., Rufford, T. E., and Hulicova-Jurcakova, D. (2015). "Poly (vinylidene fluoride) as a porogen to prepare nitrogen-enriched porous carbon electrode materials from pyrolysis of melamine resin," *Materials Today Communications* 3, 36-42. DOI: 10.1016/j.mtcomm.2015.04.001
- Gao, F., Zang, Y. H., Wang, Y., Guan, C. Q., Qu, J. Y., and Wu, M. B. (2021). "A review of the synthesis of carbon materials for energy storage from biomass and coal/heavy oil waste," *New Carbon Mater.* 36(1), 34-48. DOI: 10.1016/S1872-5805(21)60003-3
- González, A., Goikolea, E., Barrena, J. A., and Mysyk, R. (2016). "Review on supercapacitors: Technologies and materials," *Renew. Sust. Energ. Rev.* 58, 1189-1206. DOI: 10.1016/j.rser.2015.12.249
- He, X. D., Liu, Z. H., Liao, J. Y., Ding, X., Hu, Q., Xiao, L. N., Wang, S., and Chen, C. H. (2019). "A three-dimensional macroporous antimony@carbon composite as a high-performance anode material for potassium-ion batteries," *J. Mater. Chem. A* 7(16), 9629-9637. DOI: 10.1039/c9ta01968e
- Jiang, Y., He, Z., Cui, X., Liu, Z., Wan, J., Liu, Y., and Ma, F. (2022). "Hierarchical porous carbon derived from coal tar pitch by one step carbonization and activation combined with a CaO template for supercapacitors," *New J. Chem.* 46(13), 6078-6090. DOI: 10.1039/d2nj00433j
- Jin, J., Mitome, T., Egashira, Y., and Nishiyama, N. (2011). "Effect of surface area of ultramicro-, micro- and mesopores on the electric double-layer capacitance property of ordered mesoporous carbons," *J. Chem. Eng. Jpn.* 44(7), 518-523. DOI: 10.1252/jcej.11we063
- Li, Y., Wang, G., Wei, T., Fan, Z., and Yan, P. (2016). "Nitrogen and sulfur co-doped porous carbon nanosheets derived from willow catkin for supercapacitors," *Nano Energy* 19, 165-175. DOI: 10.1016/j.nanoen.2015.10.038
- Lin, C., Ritter, J. A., and Popov, B. N. (1999). "Correlation of double-layer capacitance with the pore structure of sol-gel derived carbon xerogels," *J. Electrochem. Soc.* 146(10), 3639-3643. DOI: 10.1149/1.1392526
- Lin, T., Chen, I., Liu, F., Yang, C., Bi, H., Xu, F., and Huang, F. (2015). "Nitrogen-doped mesoporous carbon of extraordinary capacitance for electrochemical energy storage," *Science* 350(6267), 1508-1513. DOI: 10.1126/science.aab3798
- Liu, R., Zhang, H., Liu, S., Zhang, X., Wu, T., Ge, X., Zang, Y., Zhao H., and Wang, G. (2016). "Shrimp-shell derived carbon nanodots as carbon and nitrogen sources to fabricate three-dimensional N-doped porous carbon electrocatalysts for the oxygen reduction reaction," *Phys. Chem. Chem. Phys.* 18(5), 4095-4101. DOI: 10.1039/c5cp06970j
- Liu, X., Liu, X., Sun, B., Zhou, H., Fu, A., Wang, Y., Guo, Y. G., Guo, P., and Li, H. (2018). "Carbon materials with hierarchical porosity: effect of template removal strategy and study on their electrochemical properties," *Carbon* 130, 680-691. DOI: 10.1016/j.carbon.2018.01.046
- Miao, L., Zhu, D., Liu, M., Duan, H., Wang, Z., Lv, Y., Xiong, W., Zhu, Q., Li, L., Chai, X., and Gan, L. (2018). "N, S co-doped hierarchical porous carbon rods derived from protic salt: facile synthesis for high energy density supercapacitors," *Electrochimica Acta* 274, 378-388. DOI: 10.1016/j.electacta.2018.04.100

- Niu, J., Shao, R., Liang, J., Dou, M., Li, Z., Huang, Y., and Wang, F. (2017). "Biomass-derived mesopore-dominant porous carbons with large specific surface area and high defect density as high performance electrode materials for Li-ion batteries and supercapacitors," *Nano Energy* 36, 322-330. DOI: 10.1016/j.nanoen.2017.04.042
- Poonam, Sharma, K., Arora, A., and Tripathi, S. K. (2019). "Review of supercapacitors: Materials and devices," *J. Energy Storage* 21, 801-825. DOI: 10.1016/j.est.2019.01.010
- Ren, R. Q., Zhong, Y., and Fan, Y. M. (2022). "A high-performance electrode based on reduced graphene oxide/lignosulfonate/carbon microspheres film for flexible supercapacitors." *BioResources* 17(1), 1729-1744. DOI: 10.15376/biores.17.1.1729-1744
- Simon, P., and Gogotsi, Y. (2020). "Perspectives for electrochemical capacitors and related devices," *Nat. Mater.* 19(11), 1151-1163. DOI: 10.1038/s41563-020-0747-z
- Shu, Y., Bai, Q., Fu, G., Xiong, Q., Li, C., Ding, H., Shen, Y., and Uyama, H. (2020). "Hierarchical porous carbons from polysaccharides carboxymethyl cellulose, bacterial cellulose, and citric acid for supercapacitor," *Carbohydr Polym* 227, 115346. DOI: 10.1016/j.carbpol.2019.115346
- Shilpa, Das, S. K., Afzal, M. A. F., Srivastava, S., Patil, S., and Sharma, A. (2016). "Enhanced electrical conductivity of suspended carbon nanofibers: Effect of hollow structure and improved graphitization," *Carbon* 108, 135-145. DOI: 10.1016/j.carbon.2016.06.103
- Song, Z., Zhu, D., Li, L., Chen, T., Duan, H., Wang, Z., Lv, Y., Xiong, W., Liu, M., and Gan, L. (2019). "Ultrahigh energy density of a N, O codoped carbon nanosphere based all-solid-state symmetric supercapacitor," *J. Mater. Chem. A* 7(3), 1177-1186. DOI: 10.1039/c8ta10158b
- Song, X. H., Chen, Q. B., Shen, E. H., and Liu, H. L. (2020). "N-doped 3D hierarchical carbon from resorcinol-formaldehyde-melamine resin for high-performance supercapacitors," *New J. Chem.* 44(20), 8638-8649. DOI: 10.1039/c9nj06415j
- Tang, H. Y., Zhao, R., Yin, H., He, D. X., and Xue, W. D. (2018). "In-situ Mg (OH)₂ template synthesis of nitrogen-doped porous carbon materials from glutinous rice for supercapacitors with excellent electrochemical performance," *Compos. Part A Appl. Sci. Manuf.* 107, 105-111. DOI: 10.1016/j.compositesa.2017.10.010
- Wang, G., Zhang, L., and Zhang, J. (2012). "A review of electrode materials for electrochemical supercapacitors," *Chem. Soc. Rev.* 41(2), 797-828. DOI: 10.1039/c1cs15060j
- Wang, L., Liu, F., Ning, Y., Bradley, R., Yang, C., Yong, K. T., Zhao, B., and Wu, W. (2020). "Biocompatible mesoporous hollow carbon nanocapsules for high performance supercapacitors," *Sci. Rep.* 10(1). DOI: 10.1038/s41598-020-61138-4
- Wen, Y., Cao, G., Cheng, J., and Yang, Y. (2005). "Correlation of capacitance with the pore structure for nanoporous glassy carbon electrodes," *J. Electrochem. Soc.* 152(9), A1770-A1775. DOI: 10.1149/1.1984447
- Xiao, P. W., Zhao, L., Sui, Z. Y., Xu, M. Y., and Han, B. H. (2017). "Direct synthesis of ordered mesoporous hydrothermal carbon materials via a modified soft-templating method," *Micropor. Mesopor. Mat.* 253, 215-222. DOI: 10.1016/j.micromeso.2017.07.001
- Xu, H., Zhang, Y., Wang, L., Chen, Y., and Gao, S. (2021). "Hierarchical porous biomass-derived carbon framework with ultrahigh surface area for outstanding

- capacitance supercapacitor,” *Renew. Energ.* 179, 1826-1835. DOI: 10.1016/j.renene.2021.08.008
- Yakaboylu, G. A., Jiang, C., Yumak, T., Zondlo, J. W., Wang, J., and Sabolsky, E. M. (2021). “Engineered hierarchical porous carbons for supercapacitor applications through chemical pretreatment and activation of biomass precursors,” *Renew. Energ.* 163, 276-287. DOI: 10.1016/j.renene.2020.08.092
- Yi, Y. J., Hou, Y., and Li, Y. M. (2020). “Preparation of high conductivity hierarchical porous carbon based on sodium lignosulfonate with pre-crosslinking,” *BioResources* 15(4), 8995-9012. DOI: 10.15376/biores.15.4.8995-9012.
- Zhang, J., Zhang, W., Zhang, H., Pang, J., Cao, G., Han, M., and Yang, Y. (2017). “A novel synthesis of hierarchical porous carbons from resol by potassium acetate activation for high performance supercapacitor electrodes,” *J. Alloy. Comp.* 712, 76-81. DOI: 10.1016/j.jallcom.2017.04.066
- Zhang, L., Hu, X., Wang, Z., Sun, F., and Dorrell, D. G. (2018). “A review of supercapacitor modeling, estimation, and applications: A control/management perspective,” *Renew. Sust. Energ. Rev.* 81, 1868-1878. DOI: 10.1016/j.rser.2017.05.283
- Zhang, P., Mu, J. H., Guo, Z. Y., Wong, S. I., Sunarso, J., Zhao, Y., Xing, W., Zhou, J. and Zhuo, S. P. (2021). “Watermelon peel-derived heteroatom-doped hierarchical porous carbon as a high-performance electrode material for supercapacitors,” *ChemElectroChem* 8(6), 1196-1203. DOI: 10.1002/celec.202100267
- Zhang, W., Cheng, R. R., Bi, H. H., Lu, Y. H., Ma, L. B., and He, X. J. (2021). “A review of porous carbons produced by template methods for supercapacitor applications,” *New Carbon Mater.* 36(1), 69-81. DOI: 10.1016/S1872-5805(21)60005-7
- Zhao, G. Y., Chen, C., Yu, D. F., Sun, L., Yang, C. H., Zhang, H., Sun, Y., Besenbacher, F., and Yu, M. (2018). “One-step production of O-N-S co-doped three-dimensional hierarchical porous carbons for high-performance supercapacitors,” *Nano Energy* 47, 547-555. DOI: 10.1016/j.nanoen.2018.03.016
- Zhou, J., Yuan, S., Lu, C., Yang, M., and Song, Y. (2020). “Hierarchical porous carbon microtubes derived from corn silks for supercapacitors electrode materials,” *J. Electroanal. Chem.* 878, article no. 114704. DOI: 10.1016/j.jelechem.2020.114704

Article submitted: August 16, 2022; Peer review completed: October 9, 2022; Revised version received: October 24, 2022; Accepted: October 25, 2022; Published: November 2, 2022.

DOI: 10.15376/biores.18.1.87-99